Atmos. Chem. Phys. Discuss., 13, 14331–14376, 2013
www.atmos-chem-phys-discuss.net/13/14331/2013/
doi:10.5194/acpd-13-14331-2013

Atmospheric Chemistry and Physics
Discussions
Open Access

Drivers of column-average CO_2 variability at Southern Hemispheric total carbon column observing network sites

N. M. Deutscher[1,2], V. Sherlock[3], S. E. Mikaloff Fletcher[3], D. W. T. Griffith[1], J. Notholt[2], R. Macatangay[1,*], B. J. Connor[4], J. Robinson[5], H. Shiona[5], V. A. Velazco[1], P. O. Wennberg[6], and D. Wunch[6]

[1]Centre for Atmospheric Chemistry, University of Wollongong, Wollongong, NSW, 2522, Australia
[2]Institute of Environmental Physics, University of Bremen, 28334 Bremen, Germany
[3]National Institute of Water and Atmospheric Research, Wellington, NZ
[4]BC Consulting, Alexandra, NZ
[5]National Institute of Water and Atmospheric Research, Lauder, NZ
[6]California Institute of Technology, Pasadena, CA, USA
[*]now at: Institute of Environmental Science and Meteorology, University of the Philippines, Diliman, Quezon City, Philippines

Received: 10 April 2013 – Accepted: 11 May 2013 – Published: 3 June 2013

Correspondence to: N. M. Deutscher (n_deutscher@iup.physik.uni-bremen.de)

Published by Copernicus Publications on behalf of the European Geosciences Union.

Abstract

We investigate factors that drive the variability in total column CO_2 at the Total Carbon Column Observing Network sites in the Southern Hemisphere using CarbonTracker analysed fluxes tagged by process and by source region. We show that the terrestrial biosphere is the largest driver of variability in the Southern Hemisphere column CO_2, however, it does not dominate in the same fashion as in the Northern Hemisphere. Local and hemispheric scale biomass burning can also play an important role, particularly at the tropical site, Darwin. The magnitude of seasonal variability in the column-average dry-air mole fraction of CO_2, X_{CO_2}, is also much smaller in the Southern Hemisphere and comparable in magnitude to the annual increase. Comparison of measurements to the model simulations highlights that there is some discrepancy between the two timeseries, especially in the early part of the Darwin data record. We show that this mismatch is most likely due to erroneously estimated local fluxes in the Australian tropical region, which are associated with enhanced photosynthesis caused by early rainfall during the tropical monsoon season.

1 Introduction

Anthropogenic emissions of carbon dioxide (CO_2) are the most important driver of human induced climate change. Understanding the temporal and spatial variability of sources and sinks of CO_2 is critical to modelling the processes that will contribute to future changes in atmospheric CO_2, anthropogenic radiative forcing and resulting climate impacts reliably. One widely used method is derived from atmospheric inverse modeling, in which estimates to the atmosphere are optimized using measurements of CO_2 (Enting and Mansbridge, 1989; Tans et al., 1990). These estimates are constrained by a relatively dense observing network on the global scale and in some regions (Peylin et al., 2013). However, several regions of importance within the carbon cycle, e.g. Siberia, South America and Africa, are poorly constrained because of a lack of measurements in those locations, as illustrated by the network of in situ sites shown in Fig. 1. In comparison to Western Europe and North America, there are also few measurements in Australasia. Altogether, this means that surface CO_2 fluxes in the Southern Hemisphere are particularly poorly constrained by in situ surface measurements.

The inference of surface fluxes from in situ measurements requires accurate modelling of atmospheric tracer transport, in particular, vertical mixing in the boundary layer and transport to the free troposphere. Errors in modelled transport are aliased into surface flux estimates. For example, Stephens et al. (2007) show that the spatial partitioning of a posteriori fluxes from inversions using a suite of transport models (but otherwise identical setups) was highly dependent on the strength of model vertical mixing.

Vertically integrated CO_2 column concentrations are less sensitive to vertical redistribution of the tracer than in situ measurements. Thus surface flux inversions based on column abundances are expected to have reduced sensitivity to errors in modelled vertical transport. Column measurements can also potentially provide information on remote locations, because they are influenced by a larger spatial area than surface in situ measurements (Keppel-Aleks et al., 2011). This comes at the expense of potentially more-detailed information about local fluxes. Quasi-global coverage of column measurements of CO_2 will be achieved via satellite platforms, such as SCIAMACHY (Burrows et al., 1995), GOSAT (Kuze et al., 2009), OCO-2 (Crisp et al., 2004) and CarbonSat (Bovensmann et al., 2010). Southern Hemisphere data from the Total Carbon Column Observing Network (TCCON) play an important role in satellite validation (e.g. Butz et al., 2011; Crisp et al., 2012; Morino et al., 2011; Reuter et al., 2011), and the low observed variability in the extra-tropical Southern Hemisphere has been exploited to derive a bias-correction for ACOS GOSAT X_{CO_2} retrievals (Wunch et al., 2011b).

Previous studies investigating X_{CO_2} in conjunction with models (e.g. Yang et al., 2007) have focused on the Northern Hemisphere. Keppel-Aleks et al. (2011) show that column measurements are influenced by hemispheric scale flux patterns, and that synoptic variability in extra-tropical Northern Hemisphere X_{CO_2} is primarily related to large-scale meridional gradients in fluxes from the terrestrial biosphere. In a subsequent study, Keppel-Aleks et al. (2012) used TCCON data to show that simulations based on unoptimised biospheric fluxes from a version of CASA underestimated the seasonal cycle magnitude in column CO_2 due to a 40 % underestimate of the strength of boreal flux seasonal cycle and a mismatch in the timing of the boreal drawdown. Houweling et al. (2010) compared four transport models driven by the same fluxes and meteorological reanalyses to four TCCON sites, including Darwin, Australia as well as the Northern Hemisphere sites Park Falls, Spitsbergen and Bremen. The comparison highlighted that the agreement in seasonal cycle shape was reasonable for the Northern Hemisphere sites, however, there was an obvious failure to reproduce the shape of seasonal cycle at Darwin in 2006 in any of the models. This suggests that there is a systematic failing in either the underlying fluxes or the transport driving these models. The models used by Houweling et al. (2010) included TM5, the model that underlies the CarbonTracker data assimilation study, and TM3, which is also used in our study.

In this study, we investigate driving factors behind variability in Southern Hemisphere X_{CO_2} measurements taken within the TCCON. This is performed via comparison of the measurements with simulations from the CarbonTracker data assimilation system (Peters et al., 2007) and a separate tagged tracer model run, both driven by the same best-estimate fluxes of CO_2 to and from the atmosphere. We investigate the processes and regions that are responsible for the simulated and measured variations in X_{CO_2}. In addition, we examine the causes of disagreement between measured and modeled timeseries of X_{CO_2}, in particular the seasonal mismatch described in Houweling et al. (2010).

The paper is laid out as follows: Sect. 2 describes the models used and Sect. 3 the measurements to which they are compared. In Sect. 4 we investigate the variability in modelled X_{CO_2} while in Sect. 5 we compare the simulations to TCCON measurements, and investigate causes of discrepancies. The conclusions follow in Sect. 6.

2 Atmospheric transport modelling

2.1 CarbonTracker 2011

The primary tool we use to investigate drivers of variability in the measured X_{CO_2} time series is the CarbonTracker (Peters et al., 2007) 2011 (hereafter "CT2011") data assimilation product, available at http://carbontracker.noaa.gov. Model CO_2 is provided on 25 or 34 vertical levels (before and after 31 December 2005, respectively) for each TCCON site. The model is run with 3° longitude × 2° latitude global resolution, with 1° × 1° "zoom" over North America. CT2011 has estimates of CO_2 fluxes to (or from) the atmosphere from biomass burning, fossil fuel emissions, the terrestrial biosphere and oceans. Details of the source of prior estimates of these fluxes are given in Table 1. In CT2011 an ensemble of prior fluxes is used, with two different estimates of each of the fossil fuel, biosphere and ocean components. The data assimilation system optimizes the terrestrial biosphere (TB) and oceanic flux (OC) components, while the fossil fuel and biomass burning components fluxes are unchanged from their prior values, described in Table 1. In the vertically resolved simulations at the TCCON sites, CO_2 total, background and process-specific mole fractions are provided every 1.5 h from 1 January 2000 to 31 December 2010. CarbonTracker uses the TM5 atmospheric transport model (Krol et al., 2005).

2.2 Tagged tracer modeling with TM3

In addition to CT2011, which provides model tracers separated by source process, we perform an additional tagged tracer model simulation to investigate regional influences. For this we use Tracer Model 3 (TM3) (Heimann and Koerner, 2003) as the atmospheric transport model. Due to an output error with the CT2011 fluxes, we use the optimized fluxes as derived for CT2010. The fluxes are run independently through the model, separated out into different tracers by process (biomass burning (BB), fossil fuel (FF), ocean (OC) and terrestrial biosphere (TB)) and by region. The regions used are largely based on the TransCom 3 regions (Gurney et al., 2002), however "Australia" is divided into 4 regions: Tropical (North of 23° S) and Temperate Australia, and the North and South Islands of New Zealand. The regions are shown in Fig. 1. This results in a total of 14 land regions and 11 ocean regions, and a global total of 53 tracers.

TM3 is an offline model that is driven by reanalysis winds. In this case, we used winds from the NCEP reanalysis project (Kalnay et al., 1996). We used the fine grid version of the model, which has a horizontal resolution of approximately 3.8° by 5° and 19 vertical levels. TM3 has been included in a wide range of model intercomparison studies (e.g. Gurney et al., 2002; Stephens et al., 2007). Stephens et al. (2007) found that TM3 was amongst the best three of the TransCom models at reproducing vertical gradients observed by aircraft profiles. Furthermore, this model has been shown to be in excellent agreement with three other models in its representation of column CO_2 at four TCCON sites, including Darwin (Houweling et al., 2010).

The model is run from 2000–2010 inclusive. With no TCCON FTIR measurements before 2004, we are able to treat the years 2000–2003 as a spin up period, allowing time for vertical and horizontal gradients to be well-established, and therefore exclude model output that pre-dates the measurement time series. We sample the model once per day, at 00:00 UT, at the locations of the TCCON sites.

TM3 simulations have been checked here for agreement with the CT2011 and CT2010 products for each source component. Both the CT2011 and TM3 time series are linearly detrended using the same linear factors, and agree to within 0.1 $\mu mol\,mol^{-1}$ on monthly timescales, not only for the total CO_2 but also for each individual process. This agreement is consistent with the previous work of Houweling et al. (2010), who compared simulations of X_{CO_2} at four TCCON stations from a wider range of models and found remarkably similar results across all of the models used, which included both TM3 and TM5. This gives us confidence in using our detrended model runs decomposed into the component regional tracers, although these simulations could still be sensitive to model biases that are common to all coarse resolution global models.

3 Measurement sites

We use measurements and simulations at the three existing Southern Hemispheric TCCON sites in Australia and New Zealand: Darwin, Wollongong and Lauder. The details for these sites are given in Table 2 and they are shown on the map in Fig. 1. Calibration of these sites occurred during the Tropical Warm Pool-International Cloud Experiment (TWP-ICE) (Darwin) (Deutscher et al., 2010) and HIaper Pole-to-Pole Observations (HIPPO) (Wofsy et al., 2011) campaigns, and agrees well with the remainder of TCCON (Wunch et al., 2010).

The sites are situated in quite different environments. Darwin, until the recent establishment of the sites at Ascension Island and Reunion Island, was the only tropical TCCON site. Wollongong and Lauder are both SH mid latitude sites, however Lauder is located inland, in a dry environment dominated by farming, while Wollongong is a coastal site close to well populated areas and industry to the north, and native forest and less dense population to the south and west. Further details about the sites, their instrumentation, uncertainties related to the data and the smoothing of the model to account for measurement a prioris and averaging kernels are given in the Appendix. As discussed in Appendix A2, we take a value of 0.4 μmol mol^{-1} to be the threshhold for a flux signature to be detectable in the TCCON measurements.

In situ FTIR analysers (Griffith et al., 2012) have been operating at Lauder since January 2007, Darwin since March 2007 and sporadically at Wollongong. However, exploring additional info on fluxes from remote, undersampled source regions using surface-column contrasts at SH TCCON sites also requires careful characterisation of in situ measurement errors. This is beyond scope of this study and will be addressed in future work.

4 Modeled variability in X_{CO_2} at SH sites

Figure 2 shows the FTS daily average time series, along with the CT2011 simulated time series, sampled at the FTS measurement times and smoothed using the TCCON a priori and averaging kernels (see Appendix A3). It is apparent that there is a yearly increase of approximately 2 µmol mol^{-1} in the model simulated time series. Also obvious is that the intra-annual variability, or seasonal cycle, is relatively small, but not fully represented in CT2011. To further investigate the magnitude of the seasonal cycles, we look now at the detrended time series for each site.

The time series are detrended by removing the average secular increase, calculated over an integer number of years, and then setting the mean of the time series to zero. The calculated trends are summarized in Table 3. We choose to use independent trends for each individual site and model time series, to encompass the different periods. The detrended time series are then used to investigate the magnitude of variability observed and expected at each site. For the model, we can examine both the total signature in X_{CO_2} and the components decomposed by process and source region. For the fossil fuel tracer, we also investigate detrending with a parabolic, rather than linear, function to account for the exponential increase in this tracer. Over the relatively short time series, the use of a parabolic fit instead of exponential causes differences of less than 0.05 µmol mol^{-1}. Neglecting the curvature, however, introduces approximately 2 µmol mol^{-1} difference to the detrended time series and significantly impacts the variability inferred in the Mean Seasonal Cycles (MSCs). To maintain the equality between the sum of the tracers and the total X_{CO_2} we detrend all tracers with a linear function, but assess the interannual variability in the fossil fuel tracer relative to a parabolic function.

Figure 3 shows the derived MSCs. These are calculated from the monthly mean of the detrended and normalized time series, averaged for each individual calendar month over multiple years. The error bars give an indication of the magnitude of the interannual variability, as determined from the standard error for each month. From top

Title Page
Abstract | Introduction
Conclusions | References
Tables | Figures
◀| |▶
◀ ▶
Back | Close
Full Screen / Esc
Printer-friendly Version
Interactive Discussion

to bottom (north to south), we can see that the magnitude of the seasonal variability in modeled X_{CO_2} gets smaller, and in all cases the amplitude is smaller than that of the yearly increase, at 0.8–1.5 µmol mol^{-1}. The magnitude of seasonal variability is quite small in comparison to the Northern Hemisphere TCCON sites such as Park Falls, Białystok and Orléans, which have a measured seasonal cycle magnitude of around 10 µmol mol^{-1} (Keppel-Aleks et al., 2011). The cycle magnitude is, however, larger than our 0.4 µmol mol^{-1} detectability criterion. Regarding the shape of the seasonal cycle, Lauder and Wollongong follow something resembling a sinusoidal pattern, with distinct (as much as can be with a small amplitude) yearly maxima and minima, and period of one year. Darwin shows more peculiar behavior, with two distinct maxima and minima each year, and the early 2006 minimum as seen in Fig. 2 in particular means that there is a large apparent measurement-model difference in DJF.

Figure 4 shows the modeled simulated MSCs for each site for CT2011, both for the total CO_2 and decomposed by source process. Data shown here are based on all model values for 2003–2010 inclusive. These are seasonal anomalies with respect to a secular trend, and the sign of the anomalies therefore does not necessarily reflect the sign of the fluxes themselves. The solid lines show the MSC in X_{CO_2} and the dots in the upper panel give the standard error in the MSC – an indication of the interannual variability (IAV) in each component.

At all three sites, the simulated contribution of the fossil fuel and ocean fluxes to variability is small, and the terrestrial biosphere signal dominates the seasonality. For Darwin, there is a significant signal due to biomass burning; the magnitude of seasonality with a late year maximum is 0.5 µmol mol^{-1}, comparable with the limit of detectability.

With respect to the IAV, the terrestrial biosphere is the largest contributor at each site. The fact that the terrestrial biosphere IAVs are generally larger than the IAV in the total X_{CO_2} implies that there is an anti-correlation between the terrestrial biosphere anomalies and those of another process or processes. The biomass burning, surprisingly, has the smallest IAV for each site, perhaps an indication that the prescribed BB fluxes do not capture the full IAV of biomass buring emissions and real variability in this flux is ascribed by the data assimilation system to the terrestrial biosphere flux. Mu et al. (2011) indeed showed that including higher frequency variability in fire emissions improved model simulations. The oceanic flux also has a small IAV.

In terms of the seasonal patterns, the bi-modal seasonality previously noted at Darwin is driven by the terrestrial biosphere and dynamics, while the other sites show more sinusoidal behavior, with maximum $X_{\mathrm{CO_2}}$ in mid-to-late Southern Hemisphere winter, also driven by the terrestrial biosphere. The other flux components serve to slightly dampen the terrestrial biosphere signal, and therefore the seasonal cycle. To investigate which region is the source of the double seasonality at Darwin, we look at the TM3 model run with the source processes further decomposed by region.

4.1 Regional decompositions

4.1.1 Terrestrial biosphere

Figure 5 shows the decomposition of the terrestrial biosphere flux signal by region. We combine all Northern Hemisphere regions except south-east Asia and combine South America and South Africa. In both cases, the shape of the MSCs from the composite regions is similar, and the aggregation serves therefore to show the net effect more clearly. For each site, the effect of the Northern Hemisphere can be clearly seen. A time lag exists between the fingerprint of the northern hemispheric biosphere at Darwin and those further south. The advection of the NH $X_{\mathrm{CO_2}}$ minimum is delayed by approximately 4 months at Darwin, and around 6 months at the extra-tropical sites. The bimodal seasonality seen at Darwin is a combination of the transport of the Northern Hemisphere flux minimum with the minimum produced from the biosphere in tropical Australia. The magnitude of the seasonality in the tropical Australian tracer is similar to that from the Northern Hemisphere, though with a less regular pattern, including a mid-year peak overlaid on a cycle that otherwise has a maximum in the Australian summer (tropical Australian wet season). In Wollongong, the significant contributors apart from the Northern Hemisphere flux are the temperate Australian region, as well as the combined South American and South African regions. The South American and South African region also imparts a noticable signal at Lauder. These model simulations indicate that under-sampled regions impart observable signatures in the SH TCCON measurements. We caution, however, that unless the error in the estimated fluxes was wrong by the magnitude of the flux, or all potential measurement biases are eliminated, these data will struggle to provide any further constraints on fluxes from these remote regions.

4.1.2 Biomass burning

Figure 6 similarly shows the breakdown by region for the biomass burning fluxes, however with a smaller vertical axis range. The magnitude of seasonality is smaller than the detectability limit in all cases, though at all sites there is evidence of a signal from the combined South American and South Africa region, with magnitude close to this detectability limit. Jones et al. (2001) have previously presented evidence of annual long-range transport of biomass burning emissions being observed at Lauder. For Darwin, a local source from tropical Australia with an October peak is also apparent. Biomass burning has a large amount of interannual variability, so in addition to looking at the MSCs, in Fig. 7 we look at the detrended time series for a few of the tracers – the South America and South Africa region for each site, and the tropical Australian and South–East Asia tracer at Darwin. The manifestation of the South America and South Africa tracer is very similar at all sites. Two years, 2007 and 2010, have seasonal cycle amplitudes that are of a magnitude that could allow them to be detected. At Darwin, the tropical Australian fire emissions show some interannual variability, with large peaks in late 2003, 2004, 2007 and 2009 and smaller peaks in other years. The South–East Asian flux is generally small, except for late 2006 when large fires occured in Indonesia (Nara et al., 2011; Paton-Walsh et al., 2010). This, and the peak years in the local fires, are of a magnitude that also could possibly be detected in the monthly mean TCCON X_{CO_2} values.

4.2 Interhemispheric transport

We have shown that Northern Hemisphere fluxes, particularly the terrestrial biosphere, play an important role in the variability of Southern Hemisphere column CO_2. One factor of interest, particularly for Darwin, which can be chemically in either the Northern or Southern Hemisphere (Hamilton et al., 2008), is the timing of interhemispheric transport. We are able to investigate this using the northern hemispheric fossil fuel tracer, because the model fossil fuel emissions have relatively small seasonal variability and therefore most variability must be due to transport driven differences. Figure 8 shows the MSC of rate of change per month of this tracer simulated at each of the Southern Hemisphere TCCON sites. The variations at Wollongong and Lauder are very similar, and only vary by a few tenths of a ppm throughout the year. Darwin, however, shows considerable within year variability, with peak transport in January and March, and almost no change in either February or April. The error bars give an indication of the interannual variability, which is generally small, but largest in the months with the correspondingly largest changes.

5 Evaluation of the simulations using TCCON

Having examined the simulated variability, and drivers thereof, in southern hemispheric column CO_2 amounts, we now compare the simulations to the measurement time series at the TCCON sites. The daily average X_{CO_2} time series are shown in Fig. 2. In general, the north-to-south latitudinal gradient between the sites is evident. Before detrending, we compare the measured and modeled trends at the sites and compare the measured and modeled time series.

The calculated trends are summarized in Table 3. To determine the trends for Wollongong and Lauder we take a simple linear fit to the monthly average measurements and model simulations. For Darwin, because of the relative irregularity of the seasonal cycle, and interannual variability in features such as the early year drawdown as seen in

Fig. 2 in 2006, we investigate various means of calculating the trend in the time series. These are the aforementioned linear fit, a linear fit excluding the early 2006 values, and a calculation based on a simple difference between months in the first (2005) and last (2010) years common to the measurement and model time series. That is, we take the average yearly change between September through December 2005 and the corresponding months in 2010. In Table 3 we also look at the global surface trend (Thomas Conway and Pieter Tans, NOAA/ESRL, www.esrl.noaa.gov/gmd/ccgg/trends/) over the time period of the FTS measurements. For Wollongong and Lauder the determined TCCON and CT2011 trends are in good agreement, certainly within the estimated uncertainties. For Darwin, the situation is more complex, but the best agreement comes from a linear fit to the data excluding early 2006. The determination based on differencing also agrees within uncertainties. The CT2011 trend is robust to all calculations, but the FTS-derived trend is more variable.

Figure 2 shows the comparison between the daily average measured and model time series, along with the difference (measurement-model mismatch) between them. The most striking feature is the failure of the model to capture the drawdown at Darwin in early 2006 and to a lesser extent in early 2007. The 2006 mismatch is quite large, reaching 3 µmol mol^{-1}. There is also some apparent pattern to the mismatch at the other two Southern Hemisphere sites, though not as pronounced as that for Darwin.

We also return to the MSCs, shown in Fig. 3. Given there are only two years of overlap, we cannot reliably interpret the Wollongong comparison. For Lauder, the agreement is to better than the detectability when averaging over multiple years. In Darwin the agreement is not quite so good, with the model underestimating the drawdown that occurs during December to February, resulting in underestimating X_{CO_2} in December, and overestimating it in January to March. This difference is on the order of the detectability limit, but is obviously strongly influenced by the years 2006 and 2007, where the difference is quite large. The error bars give an indication of the relative interannual variability between the model and measurements. The magnitude of the error bars indicates that at all sites the model predicts less interannual variability than measured.

The error bars also indicate that in Darwin there is relatively little year-to-year variation during the middle of the year, from May–September, corresponding largely to the dry season. There is considerable IAV in the early months of the year, no doubt influenced by the large drawdown apparent in 2006. In Lauder the IAV is relatively consistent throughout the year, however July and the early year exhibit larger variability. In each case, the measured IAV is greater than the detectability limit.

In evaluating the mismatches between the measurement and model time series, we refer to simulations of the dominant factors in the variability of X_{CO_2} at the Southern Hemisphere TCCON sites. Based on these, we expect that the mismatch must be driven by local or remote biosphere, or biomass burning on the local to hemispheric scale.

5.1 Local biosphere

Given the relative lack of measurements in Australia and the Southern Hemisphere in general, there is little information to increment SH fluxes in CarbonTracker if they are different from the a priori. It would therefore be unsurprising if there is a possible error in the estimate of the local biospheric flux, hence we examine the possibility for this to cause the observed disagreement. To do this, we independently run a series of regionally-tagged monthly pulse fluxes during the year of 2004, and examine their evolution in the model world at the TCCON sites. The pulses correspond to the optimized terrestrial biosphere fluxes for each region.

Figure 10 shows how the tropical Australian biosphere flux pulses are observed at all sites, normalized to their long-term effect on X_{CO_2}. Each pulse produces a maximum X_{CO_2} change of about 1.5 $\mu mol\,mol^{-1}$, with a small long-term effect of less than 0.1 $\mu mol\,mol^{-1}$. A mis-estimation of such a flux would fit well with what is seen in the mismatch – a short-term disgreement that resolves itself in a net long-term effect that is close to zero. Given the lack of measurements available to constrain the fluxes in this region, and the small net signal, the net local flux could be biased in CT2011 by a large enough amount to account for the differences. We examine the effect of the tropical Australian biosphere at the other Southern Hemisphere sites to see if they can be detected in the measurements there. Figure 10 shows the pulse signals from the Australian tropical region at Wollongong and Lauder, with smaller y-axes ranges. The signals seen here are also largest for February, but in general much smaller than the detectability limit. It is likely that such a signal, emitted from the tropics in a highly convective region, is therefore only detectable in the short-term on local spatial scales, especially as the magnitude relative to other fluxes is small. It can, however, have a large short term signal and therefore could be responsible for model-measurement mismatches observed at Darwin.

We also examine the predicted and optimized fluxes for the tropical Australian region over the course of the measurement period. Figure 11 shows the optimized terrestrial biosphere fluxes from tropical Australia for each year from 2005 to 2010. The years 2006 and 2007 have the largest January fluxes, and in no year do the fluxes increment from the prior estimate by a considerable amount. These are therefore the years that the underlying biosphere model estimates to have the largest respiration based fluxes to the atmosphere and correspond also to the years with the largest measurement-model mismatch. It is therefore very plausible that these could be overestimated fluxes, and as seen from the pulse runs, this could have a large short-term impact on the modeled columns.

The timing and magnitude of local biospheric fluxes are likely to be affected considerably by the timing of the monsoon onset. In the middle of the calendar year there is almost no rainfall, but still high temperatures. Plant photosynthesis, and hence CO_2 uptake, is known to be inhibited by water stress, and this is particularly sensitive at higher temperatures (Chaves et al., 2002). The sign of net ecosystem exchange could therefore change with the onset of the monsoon and consequent relief of water stress. Any interannual variability in the timing of the monsoon onset could therefore have an effect on the timing of the beginning of the growing season.

To examine this, we look at the rainfall measured at the Darwin ARM site, where the TCCON instrument is located. For each year from 2005–2006 to 2009–2010 we examine the cumulative rainfall between 1 October and 31 March the following year. This period is chosen to approximate the build-up and monsoon period. The cumulative rainfalls are shown in Fig. 12. 2005–2006 clearly stands out as having a much earlier significant rainfall, with more than 30 % on the total monsoonal rainfall having fallen during November 2005. This would lead to an earlier relief of water stress, and enhanced photosynthesis relative to other years, which contrasts with the prior biospheric fluxes estimated, and is a potential explanation for the mismatch between the model and the measurements. Such a change in weather is accompanied by a change in dynamics, and as a result there could be an advective signal in addition to that from the local flux. Unfortunately, no in situ CO_2 measurements were available in Darwin in 2006.

We also now look at other possible drivers of this mismatch.

5.2 Influence of the Northern Hemisphere biosphere

We previously diagnosed the influence of transport from the Northern Hemisphere using the aggregated NH fossil fuel tracer (Fig. 8). The greatest variability in transport from the Northern Hemisphere occurs for the tropical Darwin site. This variability occurs largely in the first months of the year, corresponding with the Indo-Australian monsoon season, and movement of the Intertropical Convergence Zone (ITCZ), both in the month-to-month variations, and the interannual variability for each month. The modelled transport from the Northern Hemisphere is essentially constant from month-to-month and year-to-year at Wollongong and Lauder. The consistency at these sites means that any modelled variability in other NH tracers at these sites must be due to temporal variability in the corresponding fluxes.

As previous studies have suggested that the magnitude of the seasonal cycle of biospheric uptake in boreal regions is underestimated (Keppel-Aleks et al., 2012; Yang et al., 2007), we consider this, coupled with the delay due to meridional transport, to be a candidate for causing the model overestimation in early 2006 and 2007 at Darwin.

To examine this possibility, Fig. 13 shows the manifestation of the 2004 NH boreal fluxes at Darwin. The maximum influence is considerably earlier than the timing of the mismatch, suggesting that transport of the boreal uptake period is seen in the column CO_2 data relatively quickly, within three to four months as also shown by the timing of the minimum in the Northern Hemisphere terrestrial biosphere tracer at Darwin. The SF_6 TransCom study (Denning et al., 1999) suggested that full 3-D (i.e. column) atmospheric exchange occurs about twice as fast as it manifests at the surface for TM3, and also found that TM3 had a comparatively slow interhemispheric exchange time but good agreement simulating SF_6 distributions. In addition, the total influence of the Northern Hemisphere is only on the order of $1\,\mu\text{mol}\,\text{mol}^{-1}$, so even if the strength of the uptake were to be underestimated by 40 %, which is not true for the CT2011 optimized fluxes, then the manifestation at Darwin would not result in such a large mismatch. A large underestimation of the flux would also result in a large net effect to the CO_2 time series ($0.5\,\mu\text{mol}\,\text{mol}^{-1}$ or greater) that would need to be negated by balancing in another region or via contrasting flux at another time period.

5.3 Local biomass burning

Given the interannual variability in the mismatch, biomass burning is a prime candidate for being its driver. However, the mismatch between the modeled and measured time series at Darwin sees an overestimate of the X_{CO_2} by the model. This suggests that biomass burning is not the cause of this mismatch, as in general tropical biomass burning fluxes are likely to be underestimated, due to, for example, small fires not captured in satellite fire counts or those obscured by cloud (Randerson et al., 2012). However, we investigate how well we can observe biomass burning events in the measurements.

Figure 9 shows the linearly detrended time series of X_{CO} measured by the instrument at Darwin, along with the modelled biomass burning contribution to X_{CO_2} from a combination of Australian and South–East Asian fires. In general, the timing of the features in both time series agrees well. Mu et al. (2011) previously used X_{CO} from Darwin and other sites to show that adding higher frequency variability to GFED fire emissions improved the performance of model simulations. There are regular signatures each year through September and October (and occasionally later) except in 2008. The large peak in 2006 was due to large Indonesian fires that occured that year (Paton-Walsh et al., 2010), while the other peaks all result from regular Australian savannah biomass burning. The background level in the modelled X_{CO_2} after the large 2006 fires stays enhanced relative to the measured X_{CO}, due to a persistent X_{CO_2} signal from those fires that is evident significantly longer than the atmospheric half-life of CO (~ 2 months).

The inferred emission ratio of CO/CO_2 is 0.1 mol mol^{-1}, in good agreement with previously calculated emission ratios, such as that from Andreae and Merlet (2001) of 0.10 ± 0.02 mol mol^{-1} for tropical forests and within the range of 0.050–0.130 mol mol^{-1} derived by Zhang et al. (2000) for biomass burning. They are, however lower than the 0.171 mol mol^{-1} calculated by Nara et al. (2011) for the 2006 Indonesian fires and higher than savannah burning from Andreae and Merlet (2001) and Hurst et al. (1994) of 0.06 ± 0.02 mol mol^{-1}. The emissions ratios assumed in the Global Fire Emissions Database (GFEDv3) (van der Werf et al., 2010), the source of the biomass burning fluxes in these model runs, for Indonesia and Northern Australia agree with those of Andreae and Merlet (2001) for tropical fires and savannah and grassland burning, respectively. One would expect the CO/CO_2 ratio measured here to be biased low relative to the actual emission ratio, because of the relatively shorter atmospheric lifetime of CO. Outside this event, there are a few periods of enhanced measured X_{CO} not predicted in the model X_{CO_2}, especially in 2008. In general, however, the good agreement between the measured X_{CO} and modelled biomass burning contribution to X_{CO_2} suggests that any model-data mismatch due to biomass burning is not caused by a mis-estimation of local biomass burning sources.

5.4 Remote biomass burning

Figure 7 shows that biomass burning signals from remote regions are expected to manifest themselves in similar ways at each of the three sites. Therefore, any mismatch between measurements and models should be seen similarly at all three sites, but this is not the case – the mismatches are much smaller at Lauder, while the Wollongong time series does not overlap at the time of interest. The timing of the biomass burning signal at the sites (maximum at the change of the calendar year) would have the right phase to account for the Darwin anomaly, but the magnitude is far too small to account for the differences of up to 3 µmol mol^{-1} seen.

6 Conclusions

Through assessment of CO_2 tracers tagged by region and process, we have examined the drivers of variability in X_{CO_2} at the Southern Hemisphere TCCON sites. Local and remote terrestrial biosphere are the dominant influence on changes in X_{CO_2}, but local and hemispheric-scale biomass burning can also provide signals above the limits of detectability. Comparison of model simulations with Southern Hemisphere TCCON measurements shows that the CarbonTracker data assimilation system does not capture the strong decrease in X_{CO_2} observed in the tropical monsoon season at Darwin, especially in 2006. This drawdown is associated with a monsoon season with an unusually early significant rainfall, which we propose results in early relief of water stress-limits on photosynthesis. An extended timeseries of TCCON data and surface in situ trace gas measurements at Darwin will be crucial to confirming this hypothesis. Overall, the Southern Hemisphere TCCON measurements provide additional information on CO_2 flux estimates in Australia, and the Southern Hemisphere would benefit from additional CO_2 measurements to constrain estimates of biospheric fluxes in this region.

A1 Instrumentation

All three sites are equipped with similar instrumentation: Bruker IFS125HR FTIR spectrometers. At Lauder a Bruker IFS120HR (the predecessor to the 125HR) was used from 2004 until 2010, when a 125HR instrument was commissioned and became the site's primary TCCON instrument. Spectra are simultaneously collected using two room-temperature operated detectors, Indium Gallium Arsenide (InGaAs) covering 4,000–11 000 cm^{-1} and Silicon diode (Si) covering 10 000–30 000 cm^{-1}, with the spectral range restricted to below the laser frequency (15 798 cm^{-1}) by a red filter at 15 500 cm^{-1}.

To retrieve column amounts of the gases of interest, the program suite GGG described in Wunch et al. (2011b) is used. For this analysis we use the GGG version released on 24 February 2012, hereafter referred to as GGG2012. Carbon dioxide is retrieved from the spectra in two spectral windows, centred at 6220 and 6339.5 cm^{-1}. X_{CO_2} is calculated via ratioing to the retrieved oxygen column, retrieved in a window centred at 7885 cm^{-1}. Ratioing to the atmospheric O_2 column removes uncertainties and scatter caused by effects common to both the CO_2 and O_2 retrievals, such as surface pressure variations, which would mask flux signatures in the column abundances) and some instrumental errors, such as solar tracker pointing errors (Deutscher et al., 2010; Washenfelder et al., 2006; Wunch et al., 2011a). In addition, each site uses standard TCCON procedures, including the correction for source brightness fluctuations that also reduces scatter in the retrieved X_{CO_2} (Keppel-Aleks et al., 2007).

The spectral fitting is performed using a profile scaling technique. In this method, the shape of the vertical gas profile in the atmosphere is not changed, but is scaled iteratively to provide the best match between the measured spectrum, and that calculated from the derived gas amount, instrument function and spectroscopic parameters. The shape of the gas profile is set via the a priori – for CO_2 this is a daily profile based on a climatology generated from the GLOBALVIEW product (GLOBALVIEW-CO2, 2011), changing with date and latitude. The stratospheric component of the profile is generated from the age of air relationship described by Andrews et al. (2001). The a priori profiles for each site and further details about them are given in Wunch et al. (2011b). A summary of the uncertainties associated with TCCON X_{CO_2} is also provided in Sect. 4b, Table 2 and Fig. 7 of the same publication. Prior to daily averaging, measurements are filtered based on a range of quality control criteria, including,

Title Page
Abstract Introduction
Conclusions References
Tables Figures
◂◂ ▸▸
◂ ▸
Back Close
Full Screen / Esc
Printer-friendly Version
Interactive Discussion

but not limited to, solar zenith angles less than 82° and solar intensity variation of less than five percent during the course of a scan.

A2 Data uncertainties

As a product of measurements, TCCON data are not without uncertainty. For example, despite the application of a correction for a known airmass dependent artifact (Deutscher et al., 2010; Wunch et al., 2011b), some known airmass dependent biases remain. To assess this effect, we vary the airmass corrections by ±50 % in a sensitivity study. This results in changes to the amplitude and phase of the seasonal cycle that depend on site. The maximum difference in the derived monthly means is $\pm 0.2\,\mu\text{mol}\,\text{mol}^{-1}$ at Wollongong, $\pm 0.3\,\mu\text{mol}\,\text{mol}^{-1}$ at Lauder, and smaller at Darwin due to the relatively smaller variation in airmasses observed throughout the year. Other measurement uncertainties can occur due to instrument drifts and inter-site differences as well as the simple measurement repeatability. The instrument drifts and inter-site differences are minimized by detrending the time-series and normalizing to a mean of $0\,\mu\text{mol}\,\text{mol}^{-1}$. The clear sky precision, a metric of measurement repeatability, has been estimated previously (Deutscher et al., 2010; Keppel-Aleks et al., 2007) from the standard deviation within a day as being better than $0.4\,\mu\text{mol}\,\text{mol}^{-1}$. Here, we are however interested in the ability of the measurement to capture the true average atmospheric state within a day or month, and we can therefore use the standard error to define its certainty. For daily means, and monthly means subsequently derived from the daily means, this is on average better than $0.1\,\mu\text{mol}\,\text{mol}^{-1}$. We combine this in quadrature with the uncertainty introduced by the airmass correction to yield an uncertainty of $0.32\,\mu\text{mol}\,\text{mol}^{-1}$. When looking at signals that might be detectable by these TCCON measurements, we therefore take a value larger than this, $0.4\,\mu\text{mol}\,\text{mol}^{-1}$, to constitute a detectable signal. This is a conservative estimate because it does not exploit any information about the phase of errors in the airmass correction.

A3 Comparing TCCON data to atmospheric models

When comparing the TCCON data to atmospheric model simulations, the a priori assumptions and vertical sensitivity of the retrieval need to be taken into account. This process, following the formulation of Rodgers and Connor (2003) is called smoothing, and requires knowledge of the TCCON a priori and averaging kernel. Wunch et al. (2010) recommended a slightly modified formulation because of the fact that the averaging kernels are calculated with respect to the retrieved, rather than the a priori, profile, however, the Wunch et al. and Rodgers formulations are negligibly different ($< 0.1\,\mu\text{mol}\,\text{mol}^{-1}$). The smoothed X_{CO_2} values are described by the equation:

$$c_s = c_a + h^T a^T (x_m - x_a) \tag{A1}$$

where c_s and c_a are the smoothed and a priori CO_2 columns, respectively, h describes the column summation, a is the FTS averaging kernel, in this case for CO_2 only, and x_m and x_a are the model and a priori dry-air mole fractions. The averaging kernel describes the sensitivity of the retrieved column to changes in gas amounts at each of the retrieval grid levels. Variability in TCCON averaging kernels is largely dependent on the viewing geometry – i.e. the solar zenith angle. The solar zenith angle dependence of the averaging kernels is very similar between Southern Hemisphere sites, and indeed with those network wide, as shown in Wunch et al. (2011b) for Lamont. We therefore use the standard site-independent TCCON averaging kernel product, which tabulates the averaging kernels at five degree solar zenith angle intervals. The standard product is interpolated to the measurement solar zenith angle to estimate the averaging kernel for the given measurement. We performed a sensitivity study to look at the effect of using the standard averaging kernel parameterization instead of the averaging kernels calculated for each retrieval, and the errors introduced are considerably smaller than $0.1\,\mu\text{mol}\,\text{mol}^{-1}$, even when extrapolating to low solar zenith angles at Darwin.

For each FTS measurement, we interpolate between the CT2011 model times that bracket the time of spectral collection, thereby generating a model profile corresponding to every measured CO_2 column. For comparison to the TCCON time series, we smooth the model output using the TCCON a priori and averaging kernels, following the formulation of Rodgers and Connor (2003). A smoothed model X_{CO_2} value is therefore created corresponding to each FTS X_{CO_2} measurement. In treating both the model and the measurement data in the same fashion we therefore eliminate potential biases in the comparison that could arise due to, for example, clear sky and daytime only sampling, as well as any bias that could occur from non-uniform time distribution of FTS measurements when averaging the FTS data to CT2011 time resolution. The difference in monthly means caused by the FTS sampling bias is calculated by comparing all daytime smoothed CT2011 X_{CO_2} values to those sampled at the FTS times, and the difference is less than 0.2 µmol mol^{-1}.

Acknowledgements. TCCON is funded by grant NNX11AG01G from NASA's Carbon Cycle Science Program. Measurements at Darwin are supported by Australian Research Council grant DP0879468 and NASA's Orbiting Carbon Observatory Project. The Lauder TCCON program is funded under the NZ Foundation of Research Science and Technology contracts C01X0204 and COX10406. CarbonTracker 2011 results provided by NOAA ESRL, Boulder, Colorado, USA from the website at http://carbontracker.noaa.gov. This work was also made possible by an RSNZ ISAT bilateral exchange grant and by grants from the Australian Research Council and Department of Innovation, Industry, Science and Research International Science Linkages project CG130014. Support for this work was also provided by the ESA GHG-CCI project. We gratefully acknowledge operational assistance from staff at the ARM site in Darwin.

References

Andreae, M. O. and Merlet, P.: Emission of trace gases and aerosols from biomass burning, Global Biogeochem. Cy., 15, 955–966, doi:10.1029/2000GB001382, 2001. 14349

Andrews, A., Boering, K., Daube, B., Wofsy, S., Loewenstein, M., Jost, H., Podolske, J., Webster, C., Herman, R., Scott, D., Flesch, G., Moyer, E., Elkins, J., Dutton, G., Hurst, D., Moore, F., Ray, E., Romashkin, P., and Strahan, S.: Mean ages of stratospheric air derived from in situ observations of CO_2, CH_4, and N_2O, J. Geophys. Res., 106, 32295–32314, doi:10.1029/2001JD000465, 2001. 14351

Bovensmann, H., Buchwitz, M., Burrows, J. P., Reuter, M., Krings, T., Gerilowski, K., Schneising, O., Heymann, J., Tretner, A., and Erzinger, J.: A remote sensing technique for global monitoring of power plant CO_2 emissions from space and related applications, Atmos. Meas. Tech., 3, 781–811, doi:10.5194/amt-3-781-2010, 2010. 14334

Burrows, J., Holzle, E., Goede, A., Visser, H., and Fricke, W.: Sciamachy – scanning imaging absorption spectrometer for atmospheric chartography, Acta Astronaut., 35, 445–451, doi:10.1016/0094-5765(94)00278-T, 1995. 14334

Butz, A., Guerlet, S., Hasekamp, O., Schepers, D., Galli, A., Aben, I., Frankenberg, C., Hartmann, J.-M., Tran, H., Kuze, A., Keppel-Aleks, G., Toon, G., Wunch, D., Wennberg, P., Deutscher, N., Griffith, D., Macatangay, R., Messerschmidt, J., Notholt, J., and Warneke, T.: Toward accurate CO_2 and CH_4 observations from GOSAT, Geophys. Res. Lett., 38, L14812, doi:10.1029/2011GL047888, 2011. 14334

Chaves, M., Pereira, J., Maroco, J., Rodrigues, M., Ricardo, C., Osorio, M., Carvalho, I., Faria, T., and Pinheiro, C.: How plants cope with water stress in the field. Photosynthesis and growth, Ann. Bot., 89, 907–916, doi:10.1093/aob/mcf105, 2002. 14346

Crisp, D., Atlas, R. M., Breon, F. M., Brown, L. R., Burrows, J. P., Ciais, P., Connor, B. J., Doney, S. C., Fung, I. Y., Jacob, D. J., Miller, C. E., O'Brien, D., Pawson, S., Randerson, J. T., Rayner, P., Salawitch, R. J., Sander, S. P., Sen, B., Stephens, G. L., Tans, P. P., Toon, G. C., Wennberg, P. O., Wofsy, S. C., Yung, Y. L., Kuang, Z., Chudasama, B., Sprague, G., Weiss, B., Pollock, R., Kenyon, D., and Schroll, S.: The Orbiting Carbon Observatory (OCO) mission, Adv. Space Res., 34, 700–709, http://www.sciencedirect.com/science/article/pii/S0273117704003539, 2004. 14334

Crisp, D., Fisher, B. M., O'Dell, C., Frankenberg, C., Basilio, R., Bösch, H., Brown, L. R., Castano, R., Connor, B., Deutscher, N. M., Eldering, A., Griffith, D., Gunson, M., Kuze, A., Mandrake, L., McDuffie, J., Messerschmidt, J., Miller, C. E., Morino, I., Natraj, V., Notholt, J., O'Brien, D. M., Oyafuso, F., Polonsky, I., Robinson, J., Salawitch, R., Sherlock, V., Smyth, M., Suto, H., Taylor, T. E., Thompson, D. R., Wennberg, P. O., Wunch, D., and Yung, Y. L.: The ACOS CO_2 retrieval algorithm – Part II: Global X_{CO_2} data characterization, Atmos. Meas. Tech., 5, 687–707, doi:10.5194/amt-5-687-2012, 2012. 14334

Denning, A. S., Holzer, M., Gurney, K. R., Heimann, M., Law, R. M., Rayner, P. J., Fung, I. Y., Fan, S.-M., Taguchi, S., Friedlingstein, P., Balkanski, Y., Taylor, J., Maiss, M., and Levin, I.: Three-dimensional transport and concentration of SF6, Tellus B, 51, 266–297, doi:10.1034/j.1600-0889.1999.00012.x, 1999. 14348

Deutscher, N. M., Griffith, D. W. T., Bryant, G. W., Wennberg, P. O., Toon, G. C., Washenfelder, R. A., Keppel-Aleks, G., Wunch, D., Yavin, Y., Allen, N. T., Blavier, J.-F., Jiménez, R., Daube, B. C., Bright, A. V., Matross, D. M., Wofsy, S. C., and Park, S.: Total column CO_2 measurements at Darwin, Australia – site description and calibration against in situ aircraft profiles, Atmos. Meas. Tech., 3, 947–958, doi:10.5194/amt-3-947-2010, 2010. 14338, 14351, 14352

Enting, I. G. and Mansbridge, J. V.: Seasonal sources and sinks of atmospheric CO(2) Direct inversion of filtered data, Tellus B, 41, 111–126, doi:10.1111/j.1600-0889.1989.tb00129.x, 1989. 14333

GLOBALVIEW-CO2: Cooperative Atmospheric Data Integration Project – Carbon Dioxide, CD-ROM, also available on Internet via anonymous FTP to ftp://ftp.cmdl.noaa.gov, Path: ccg/co2/GLOBALVIEW, 2011. 14351

Griffith, D. W. T., Deutscher, N. M., Caldow, C., Kettlewell, G., Riggenbach, M., and Hammer, S.: A Fourier transform infrared trace gas and isotope analyser for atmospheric applications, Atmos. Meas. Tech., 5, 2481–2498, doi:10.5194/amt-5-2481-2012, 2012. 14338

Gurney, K. R., Law, R. M., Denning, A. S., Rayner, P. J., Baker, D., Bousquet, P., Bruhwiler, L., Chen, Y.-H., Ciais, P., Fan, S., Fung, I. Y., Gloor, M., Heimann, M., Higuchi, K., John, J., Maki, T., Maksyutov, S., Masarie, K., Peylin, P., Prather, M., Pak, B. C., Randerson, J., Sarmiento, J., Taguchi, S., Takahashi, T., and Yuen, C.-W.: Towards robust regional estimates of CO_2 sources and sinks using atmospheric transport models, Nature, 415, 626–630, doi:10.1038/415626a, 2002. 14337

Hamilton, J. F., Allen, G., Watson, N. M., Lee, J. D., Saxton, J. E., Lewis, A. C., Vaughan, G., Bower, K. N., Flynn, M. J., Crosier, J., Carver, G. D., Harris, N. R. P., Parker, R. J., Remedios, J. J., and Richards, N. A. D.: Observations of an atmospheric chemical equator and its implications for the tropical warm pool region, J. Geophys. Res.-Atmos., 113, D20313, doi:10.1029/2008JD009940, 2008. 14343

Heimann, M. and Koerner, S.: The global atmospheric tracer model TM3, Tech. Rep. 5, Max-Planck-Institut fuer Biogeochemie, Jena, Germany, 2003. 14336

Houweling, S., Aben, I., Breon, F.-M., Chevallier, F., Deutscher, N., Engelen, R., Gerbig, C., Griffith, D., Hungershoefer, K., Macatangay, R., Marshall, J., Notholt, J., Peters, W., and Serrar, S.: The importance of transport model uncertainties for the estimation of CO_2

sources and sinks using satellite measurements, Atmos. Chem. Phys., 10, 9981–9992, doi:10.5194/acp-10-9981-2010, 2010. 14335, 14337

Hurst, D., Griffith, D., Carras, J., Williams, D., and Fraser, P.: Measurements of trace gases emitted by Australian savanna fires during the 1990 dry season, J. Atmos. Chem., 18, 33–56, doi:10.1007/BF00694373, 1994. 14349

Jacobson, A. R., Mikaloff Fletcher, S. E., Gruber, N., Sarmiento, J. L., and Gloor, M.: A joint atmosphere-ocean inversion for surface fluxes of carbon dioxide: 1. Methods and global-scale fluxes, Global Biogeochem. Cy., 21, GB1019, doi:10.1029/2005GB002556, 2007. 14361

Jones, N., Rinsland, C., Liley, J., and Rosen, J.: Correlation of aerosol and carbon monoxide at 45 degrees S: evidence of biomass burning emissions, Geophys. Res. Lett., 28, 709–712, doi:10.1029/2000GL012203, 2001. 14342

Kalnay, E., Kanamitsu, M., Kistler, R., Collins, W., Deaven, D., Gandin, L., Iredell, M., Saha, S., White, G., Woollen, J., Zhu, Y., Leetmaa, A., Reynolds, R., Chelliah, M., Ebisuzaki, W., Higgins, W., Janowiak, J., Mo, K. C., Ropelewski, C., Wang, J., Jenne, R., and Joseph, D.: The NCEP/NCAR 40-Year Reanalysis Project, B. Amer. Meteorol. Soc., 77, 437–471, doi:10.1175/1520-0477(1996)077<0437:TNYRP>2.0.CO;2, 1996. 14337

Keppel-Aleks, G., Toon, G. C., Wennberg, P. O., and Deutscher, N. M.: Reducing the impact of source brightness fluctuations on spectra obtained by Fourier-transform spectrometry, Appl. Opt., 46, 4774–4779, 2007. 14351, 14352

Keppel-Aleks, G., Wennberg, P. O., and Schneider, T.: Sources of variations in total column carbon dioxide, Atmos. Chem. Phys., 11, 3581–3593, doi:10.5194/acp-11-3581-2011, 2011. 14334, 14340

Keppel-Aleks, G., Wennberg, P. O., Washenfelder, R. A., Wunch, D., Schneider, T., Toon, G. C., Andres, R. J., Blavier, J.-F., Connor, B., Davis, K. J., Desai, A. R., Messerschmidt, J., Notholt, J., Roehl, C. M., Sherlock, V., Stephens, B. B., Vay, S. A., and Wofsy, S. C.: The imprint of surface fluxes and transport on variations in total column carbon dioxide, Biogeosciences, 9, 875–891, doi:10.5194/bg-9-875-2012, 2012. 14335, 14347

Krol, M., Houweling, S., Bregman, B., van den Broek, M., Segers, A., van Velthoven, P., Peters, W., Dentener, F., and Bergamaschi, P.: The two-way nested global chemistry-transport zoom model TM5: algorithm and applications, Atmos. Chem. Phys., 5, 417–432, doi:10.5194/acp-5-417-2005, 2005. 14336

Kuze, A., Suto, H., Nakajima, M., and Hamazaki, T.: Thermal and near infrared sensor for carbon observation Fourier-transform spectrometer on the Greenhouse Gases Observing Satellite for greenhouse gases monitoring, Appl. Opt., 48, 6716–6733, 2009. 14334

Morino, I., Uchino, O., Inoue, M., Yoshida, Y., Yokota, T., Wennberg, P. O., Toon, G. C., Wunch, D., Roehl, C. M., Notholt, J., Warneke, T., Messerschmidt, J., Griffith, D. W. T., Deutscher, N. M., Sherlock, V., Connor, B., Robinson, J., Sussmann, R., and Rettinger, M.: Preliminary validation of column-averaged volume mixing ratios of carbon dioxide and methane retrieved from GOSAT short-wavelength infrared spectra, Atmos. Meas. Tech., 4, 1061–1076, doi:10.5194/amt-4-1061-2011, 2011. 14334

Mu, M., Randerson, J. T., van der Werf, G. R., Giglio, L., Kasibhatla, P., Morton, D., Collatz, G. J., DeFries, R. S., Hyer, E. J., Prins, E. M., Griffith, D. W. T., Wunch, D., Toon, G. C., Sherlock, V., and Wennberg, P. O.: Daily and 3-hourly variability in global fire emissions and consequences for atmospheric model predictions of carbon monoxide, J. Geophys. Res.-Atmos., 116, D24303, doi:10.1029/2011JD016245, 2011. 14341, 14348

Nara, H., Tanimoto, H., Nojiri, Y., Mukai, H., Zeng, J., Tohjima, Y., and Machida, T.: CO emissions from biomass burning in South-east Asia in the 2006 El Niño year: shipboard and AIRS satellite observations, Environ. Chem., 8, 213–223, doi:10.1071/EN10113, 2011. 14342, 14349

Oda, T. and Maksyutov, S.: A very high-resolution (1 km × 1 km) global fossil fuel CO_2 emission inventory derived using a point source database and satellite observations of nighttime lights, Atmos. Chem. Phys., 11, 543–556, doi:10.5194/acp-11-543-2011, 2011. 14361

Paton-Walsh, C., Deutscher, N. M., Griffith, D. W. T., Forgan, B. W., Wilson, S. R., Jones, N. B., and Edwards, D. P.: Trace gas emissions from savanna fires in northern Australia, J. Geophys. Res., 115, D16314, doi:10.1029/2009JD013309, 2010. 14342, 14349

Peters, W., Jacobson, A. R., Sweeney, C., Andrews, A. E., Conway, T. J., Masarie, K., Miller, J. B., Bruhwiler, L. M. P., Pétron, G., Hirsch, A. I., Worthy, D. E. J., van der Werf, G. R., Randerson, J. T., Wennberg, P. O., Krol, M. C., and Tans, P. P.: An atmospheric perspective on North American carbon dioxide exchange: CarbonTracker, P. Natl. Acad. Sci. USA, 104, 18925–18930, doi:10.1073/pnas.0708986104, 2007. 14335, 14336

Peylin, P., Law, R. M., Gurney, K. R., Chevallier, F., Jacobson, A. R., Maki, T., Niwa, Y., Patra, P. K., Peters, W., Rayner, P. J., Rödenbeck, C., and Zhang, X.: Global atmospheric carbon budget: results from an ensemble of atmospheric CO_2 inversions, Biogeosciences Discuss., 10, 5301–5360, doi:10.5194/bgd-10-5301-2013, 2013. 14333

Randerson, J. T., Chen, Y., van der Werf, G. R., Rogers, B. M., and Morton, D. C.: Global burned area and biomass burning emissions from small fires, J. Geophys. Res., 117, G04012, doi:10.1029/2012JG002128, 2012. 14348

Reuter, M., Bovensmann, H., Buchwitz, M., Burrows, J. P., Connor, B. J., Deutscher, N. M., Griffith, D. W. T., Heymann, J., Keppel-Aleks, G., Messerschmidt, J., Notholt, J., Petri, C., Robinson, J., Schneising, O., Sherlock, V., Velazco, V., Warneke, T., Wennberg, P. O., and Wunch, D.: Retrieval of atmospheric CO_2 with enhanced accuracy and precision from SCIAMACHY: Validation with FTS measurements and comparison with model results, J. Geophys. Res., 116, D04301, doi:10.1029/2010JD015047, 2011. 14334

Rodgers, C. D. and Connor, B. J.: Intercomparison of remote sounding instruments, J. Geophys. Res., 108, 4116, doi:10.1029/2002JD002299, 2003. 14353, 14354

Stephens, B. B., Gurney, K. R., Tans, P. P., Sweeney, C., Peters, W., Bruhwiler, L., Ciais, P., Ramonet, M., Bousquet, P., Nakazawa, T., Aoki, S., Machida, T., Inoue, G., Vinnichenko, N., Lloyd, J., Jordan, A., Heimann, M., Shibistova, O., Langenfelds, R. L., Steele, L. P., Francey, R. J., and Denning, A. S.: Weak northern and strong tropical land carbon uptake from vertical profiles of atmospheric CO_2, Science, 316, 1732–1735, doi:10.1126/science.1137004, 2007. 14334, 14337

Takahashi, T., Sutherland, S. C., Wanninkhof, R., Sweeney, C., Feely, R. A., Chipman, D. W., Hales, B., Friederich, G., Chavez, F., Sabine, C., Watson, A., Bakker, D. C. E., Schuster, U., Metzl, N., Yoshikawa-Inoue, H., Ishii, M., Midorikawa, T., Nojiri, Y., Koertzinger, A., Steinhoff, T., Hoppema, M., Olafsson, J., Arnarson, T. S., Tilbrook, B., Johannessen, T., Olsen, A., Bellerby, R., Wong, C. S., Delille, B., Bates, N. R., and de Baar, H. J. W.: Climatological mean and decadal change in surface ocean $p\mathrm{CO}_2$, and net sea-air CO_2 flux over the global oceans, Deep-Sea Res. Pt II, 56, 554–577, doi:10.1016/j.dsr2.2008.12.009, 2009. 14361

Tans, P., Fung, I., and Takahashi, T.: Observational constraints on the global atmospheric CO_2 budget, Science, 247, 1431–1438, doi:10.1126/science.247.4949.1431, 1990. 14333

van der Werf, G. R., Randerson, J. T., Giglio, L., Collatz, G. J., Mu, M., Kasibhatla, P. S., Morton, D. C., DeFries, R. S., Jin, Y., and van Leeuwen, T. T.: Global fire emissions and the contribution of deforestation, savanna, forest, agricultural, and peat fires (1997–2009), Atmos. Chem. Phys., 10, 11707–11735, doi:10.5194/acp-10-11707-2010, 2010. 14349

Washenfelder, R. A., Toon, G. C., Blavier, J.-F., Yang, Z., Allen, N. T., Wennberg, P. O., Vay, S. A., Matross, D. M., and Daube, B. C.: Carbon dioxide column abundances at the Wisconsin Tall Tower site, J. Geophys. Res., 111, D22305, doi:10.1029/2006JD007154, 2006. 14351

Wofsy, S. C., Team, H. S., Team, C. M., and Team, S.: HIAPER Pole-to-Pole Observations (HIPPO): fine-grained, global-scale measurements of climatically important atmospheric gases and aerosols, Philos. Trans. Roy. Soc. A, 369, 2073–2086, doi:10.1098/rsta.2010.0313, 2011. 14338

Wunch, D., Toon, G. C., Wennberg, P. O., Wofsy, S. C., Stephens, B. B., Fischer, M. L., Uchino, O., Abshire, J. B., Bernath, P., Biraud, S. C., Blavier, J.-F. L., Boone, C., Bowman, K. P., Browell, E. V., Campos, T., Connor, B. J., Daube, B. C., Deutscher, N. M., Diao, M., Elkins, J. W., Gerbig, C., Gottlieb, E., Griffith, D. W. T., Hurst, D. F., Jiménez, R., Keppel-Aleks, G., Kort, E. A., Macatangay, R., Machida, T., Matsueda, H., Moore, F., Morino, I., Park, S., Robinson, J., Roehl, C. M., Sawa, Y., Sherlock, V., Sweeney, C., Tanaka, T., and Zondlo, M. A.: Calibration of the Total Carbon Column Observing Network using aircraft profile data, Atmos. Meas. Tech., 3, 1351–1362, doi:10.5194/amt-3-1351-2010, 2010. 14338, 14353

Wunch, D., Toon, G. C., Blavier, J. F. L., Washenfelder, R. A., Notholt, J., Connor, B. J., Griffith, D. W. T., Sherlock, V., and Wennberg, P. O.: The total carbon column observing network, Philos. Trans. Roy. Soc. A, 369, 2087–2112, doi:10.1098/rsta.2010.0240, 2011a. 14351

Wunch, D., Wennberg, P. O., Toon, G. C., Connor, B. J., Fisher, B., Osterman, G. B., Frankenberg, C., Mandrake, L., O'Dell, C., Ahonen, P., Biraud, S. C., Castano, R., Cressie, N., Crisp, D., Deutscher, N. M., Eldering, A., Fisher, M. L., Griffith, D. W. T., Gunson, M., Heikkinen, P., Keppel-Aleks, G., Kyrö, E., Lindenmaier, R., Macatangay, R., Mendonca, J., Messerschmidt, J., Miller, C. E., Morino, I., Notholt, J., Oyafuso, F. A., Rettinger, M., Robinson, J., Roehl, C. M., Salawitch, R. J., Sherlock, V., Strong, K., Sussmann, R., Tanaka, T., Thompson, D. R., Uchino, O., Warneke, T., and Wofsy, S. C.: A method for evaluating bias in global measurements of CO_2 total columns from space, Atmos. Chem. Phys., 11, 12317–12337, doi:10.5194/acp-11-12317-2011, 2011b. 14334, 14351, 14352, 14353

Yang, Z., Washenfelder, R. A., Keppel-Aleks, G., Krakauer, N. Y., Randerson, J. T., Tans, P. P., Sweeney, C., and Wennberg, P. O.: New constraints on Northern Hemisphere growing season net flux, Geophys. Res. Lett., 34, L12807, doi:10.1029/2007GL029742, 2007. 14334, 14347

Zhang, J., Smith, K. R., Ma, Y., Ye, S., Jiang, F., Qi, W., Liu, P., Khalil, M. A. K., Rasmussen, R. A., and Thorneloe, S. A.: Greenhouse gases and other airborne pollutants from household stoves in China: a database for emission factors, Atmos. Environ., 34, 4537–4549, doi:10.1016/S1352-2310(99)00450-1, 2000. 14349

Table 1. Details of CT2011 prior and posterior fluxes used in this comparison.

Flux	Source of prior flux	Optimized (Yes/No)
Biomass burning (BB)	GFED-CASAv3	No
Fossil fuel (FF)	CDIAC extended to 2009–2010 via 2011 BP energy consumption statistics ODIAC (Oda and Maksyutov, 2011) extended to 2008–2010 via 2011 BP energy consumption statistics	No No
Ocean (OC)	Jacobson et al. (2007) pCO_2 based on Takahashi et al. (2009)	Yes Yes
Terrestrial biosphere (TB)	GFED-CASAv2 GFED-CASAv3	Yes Yes

Table 2. Sites used in this study

Site	Latitude (˚S)	Longitude (˚E)	Altitude (m a.s.l.)	Instrument	Measurement years
Darwin	12.425	130.891	30	125HR	Aug 2005–present
Wollongong	34.406	150.879	30	125HR	May 2008–present
Lauder	45.038	169.684	370	120HR 125HR	2004–present 2010–present

Table 3. Comparison of yearly trends between FTS measurements and CT2011 smoothed column X_{CO_2}. All values are given in μmol mol^{-1} yr^{-1} ± standard deviation.

Site	FTS trend	CT2011 trend	Global surface trend
Darwin	2.17 ± 0.08	1.93 ± 0.05	1.96
	1.85 ± 0.10	1.98 ± 0.07	from monthly differences
	2.01 ± 0.07	1.92 ± 0.06	excluding Jan–Jun 2006
Wollongong	1.75 ± 0.16	1.79 ± 0.11	2.02*
Lauder	1.84 ± 0.04	1.86 ± 0.04	1.96

* Calculated from the integer years 2009 and 2010.

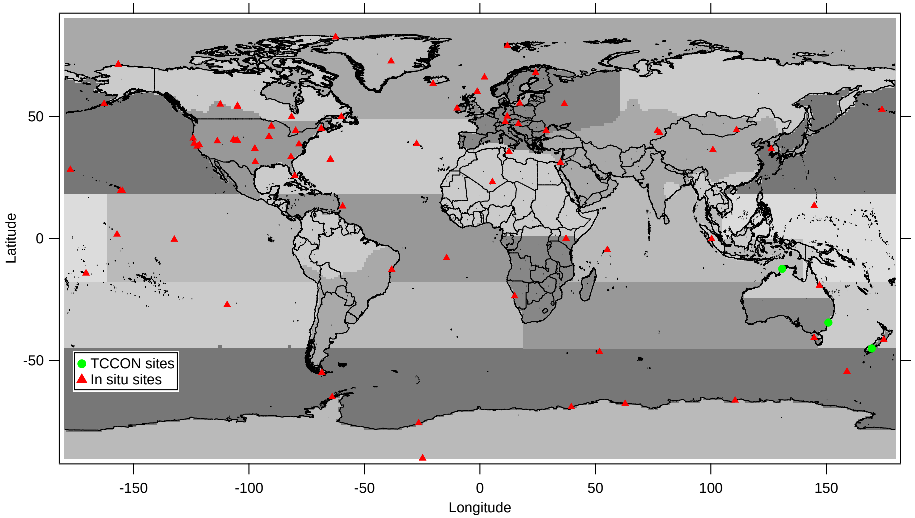

Fig. 1. A world map showing the TCCON sites used in this study (green circles), other in situ sampling sites (red triangles) and the model aggregation regions used in this study, which are based on the TransCom regions.

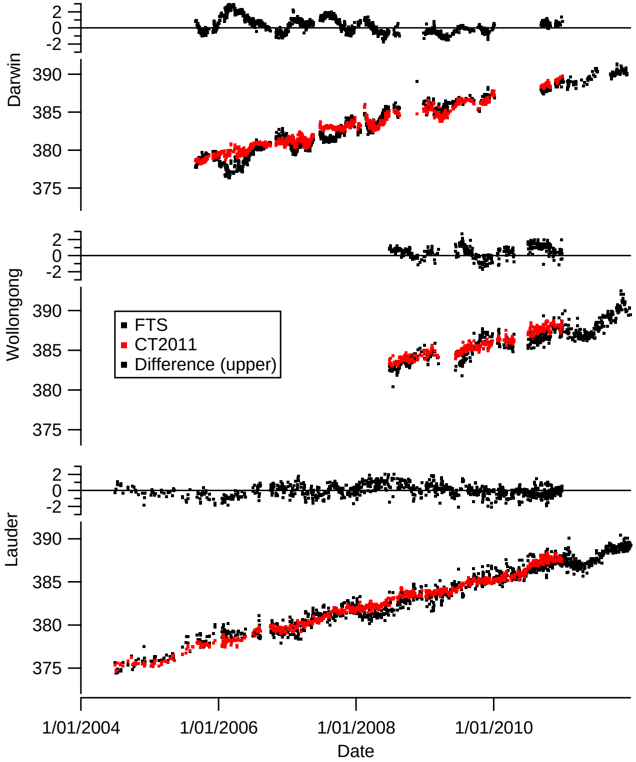

Fig. 2. Measured (black) and CT2011 modeled (red) daily average time series of X_{CO_2} at the three Southern Hemisphere TCCON sites. For each site, the difference between the modeled and measured (measured–modeled) values is given in a separate panel. The model output are interpolated to the times of the FTS measurements, and then smoothed with the FTS a priori and averaging kernel profiles.

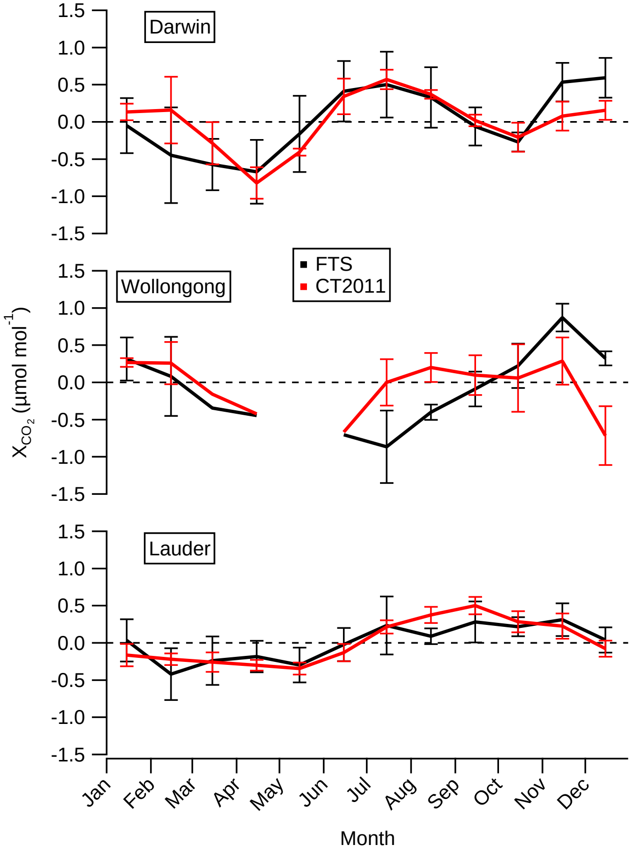

Fig. 3. Derived Mean Seasonal Cycles for the FTS (black) and CT2011 (red) time series for each site. The error bars are derived from the standard deviation of the mean difference within each month from a secular trend, and give an indication of the interannual variability. For Darwin, the MSC is derived from 2006–2010 inclusive, for Lauder 2005–2010 and Wollongong from only 2009–2010.

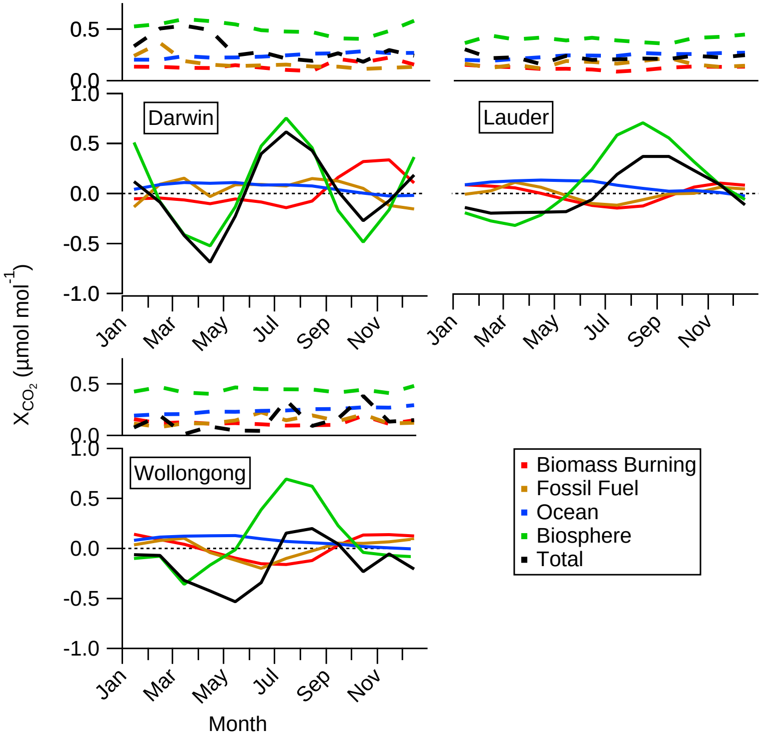

Fig. 4. Mean seasonal cycles in the CT2011 simulation for the Southern Hemisphere TCCON sites Darwin (top left), Wollongong (bottom) and Lauder (top right), decomposed by source process: total (black), biomass burning (red), ocean (blue), terrestrial biosphere (green) and fossil fuel (brown). For each site the magnitude of the interannual variability (as derived from the standard deviation in the derived Mean seasonal cycle) is given by the dashed lines in the upper panel, with colors corresponding to the individual flux components shown by the solid lines in the lower panel.

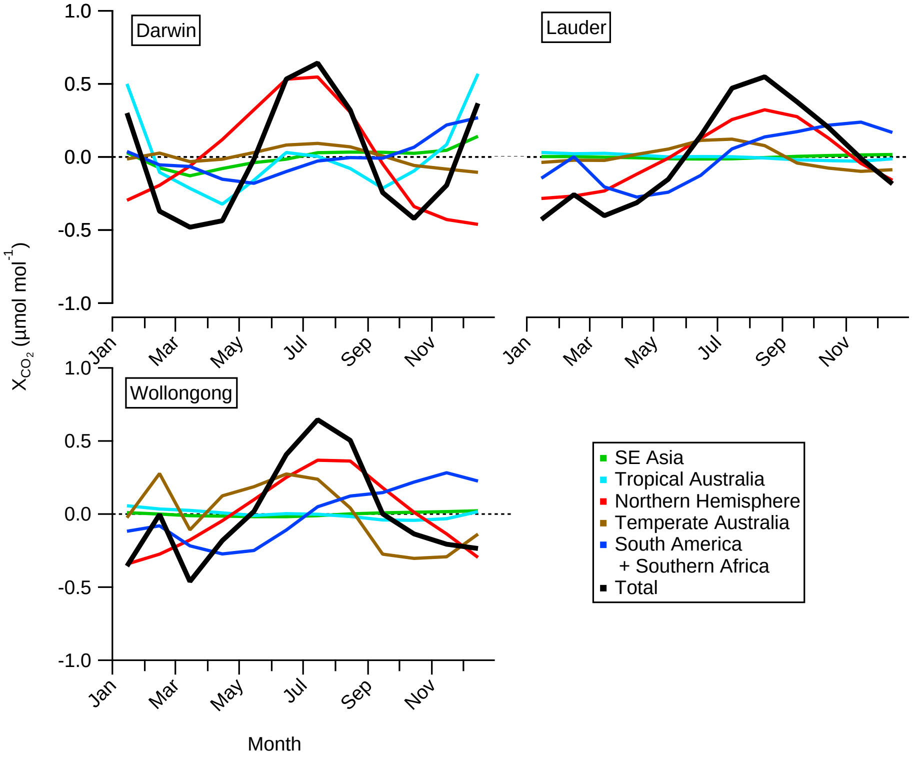

Fig. 5. Regional decomposition of the mean seasonal cycles of the terrestrial biosphere in the TM3 simulation with CT2010 fluxes.

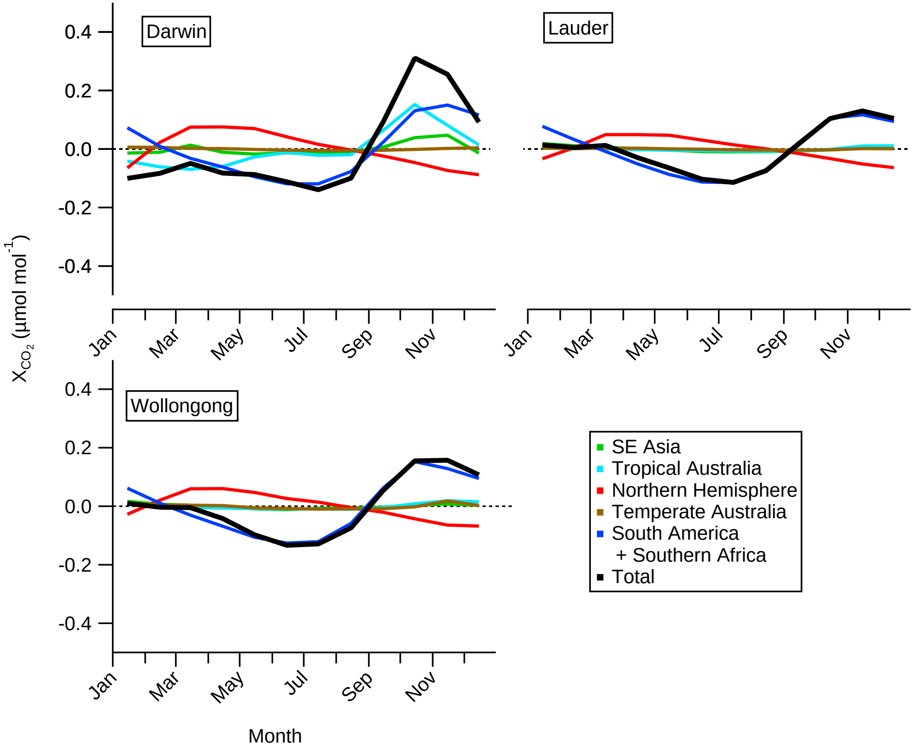

Fig. 6. Regional decomposition of the mean seasonal cycles of biomass burning in the TM3 simulation with CT2010 fluxes.

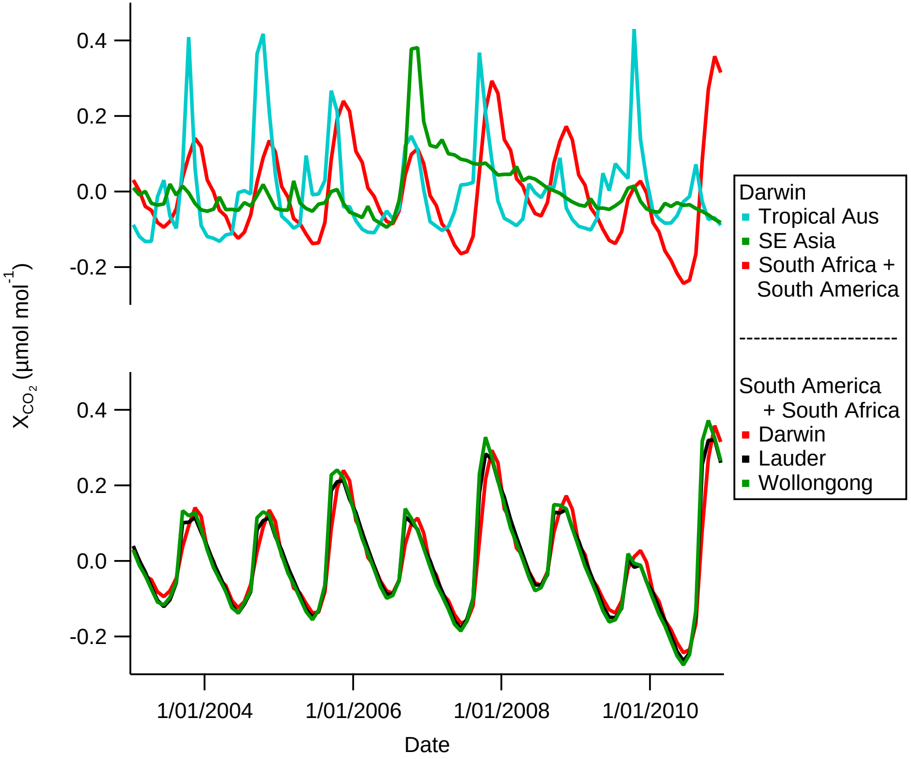

Fig. 7. Time series of regional decomposition of the detrended time series for the South American and South African biomass burning tracer at all three sites and the tropical Australian and South-East Asian tracers as sampled at Darwin.

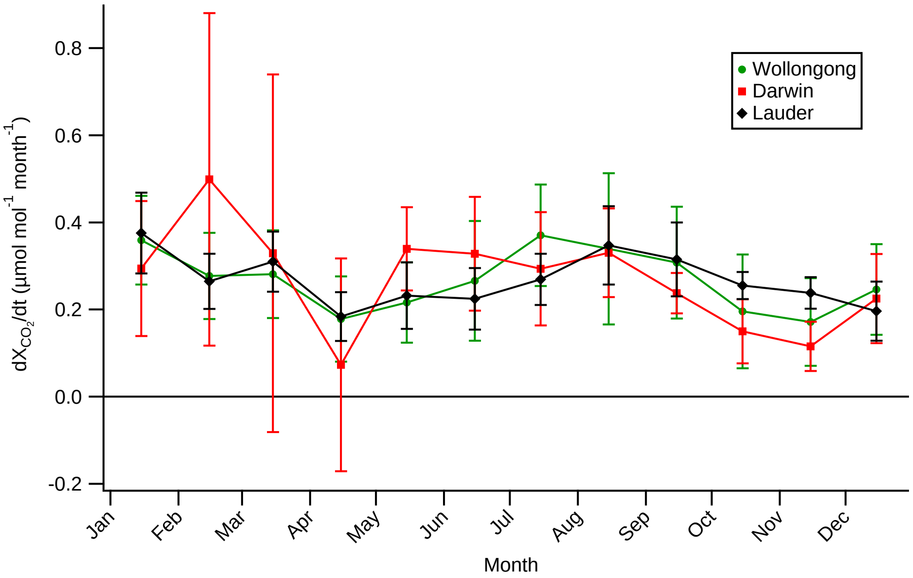

Fig. 8. Mean seasonal cycles of the change in the Northern Hemisphere fossil fuel tracer per month simulated at each of the Southern Hemisphere TCCON sites. The error bars are equal to two standard deviations about the mean.

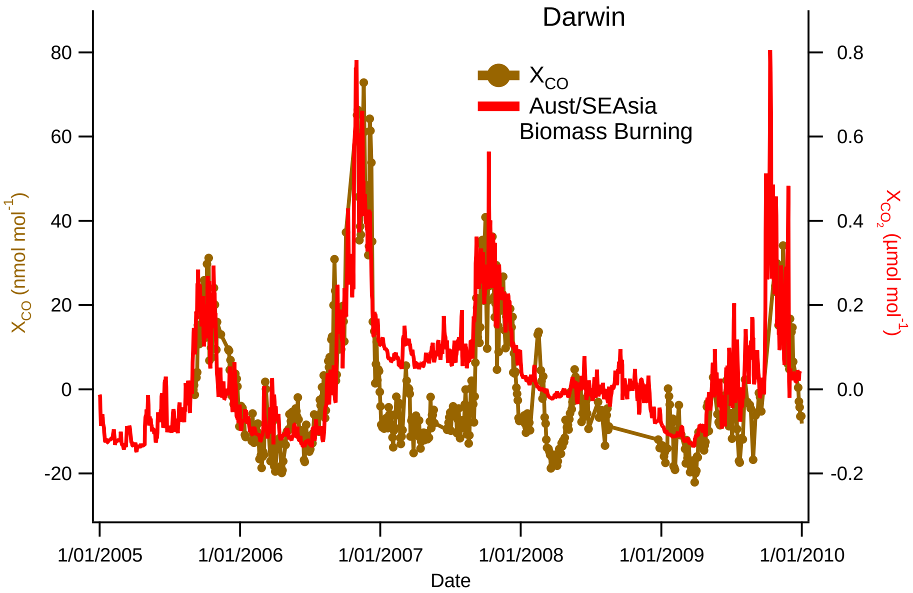

Fig. 9. Linearly detrended time series of X_{CO} measured by the TCCON FTS at Darwin (brown) and the modelled contribution of local (Australian and South-East Asian) biomass burning to the X_{CO_2} (red).

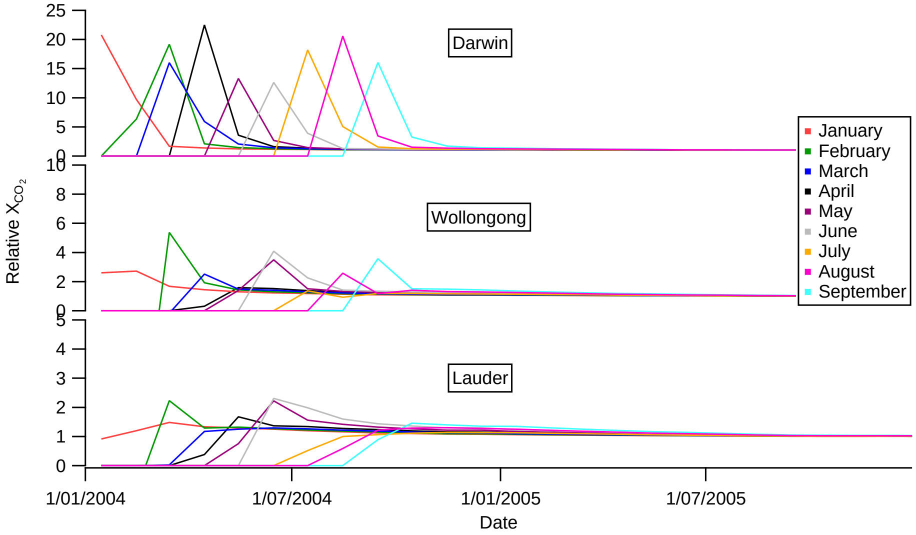

Fig. 10. The time series of relative X_{CO_2} changes resulting from each month's terrestrial biosphere flux in the tropical Australian region. The X_{CO_2} values are normalized to the long-term value caused by the pulse in question and therefore are always positive, and indicate the relative ability of a flux from a particular month to affect the X_{CO_2}. The effect of each month's terrestrial biosphere flux reaches a maximum X_{CO_2} contribution of 1.5 µmol mol^{-1} with a long-term effect of less than 0.1 µmol mol^{-1}.

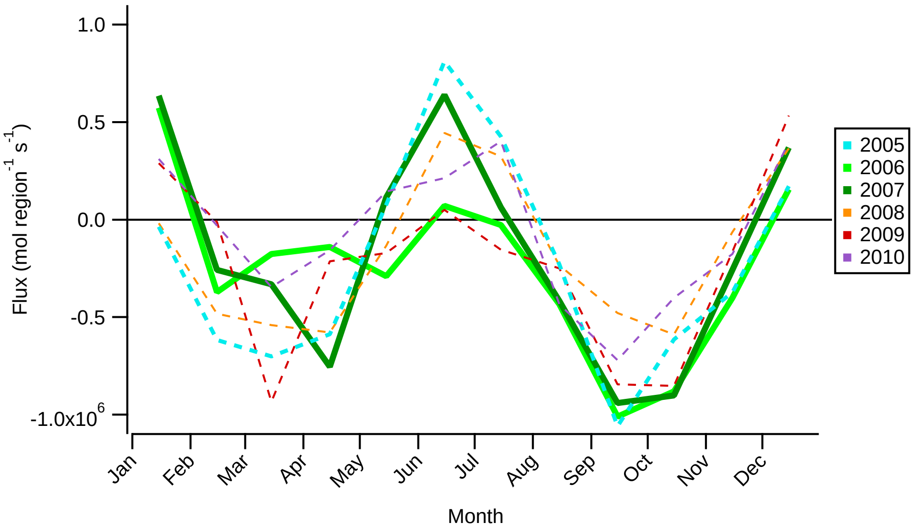

Fig. 11. The optimized tropical Australian terrestrial biosphere fluxes for each year from 2005 to 2010.

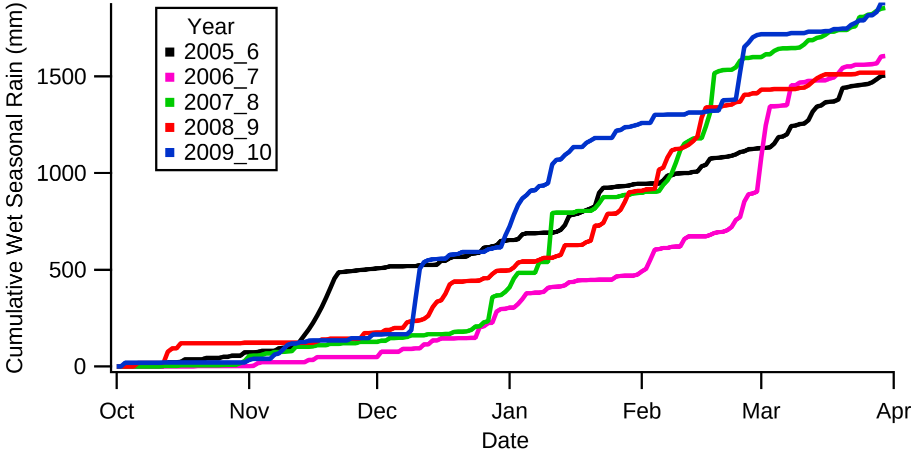

Fig. 12. Cumulative rainfall through each monsoon season (October through to the following March) from 2005–2006 to 2009–2010 as measured at the ARM site.

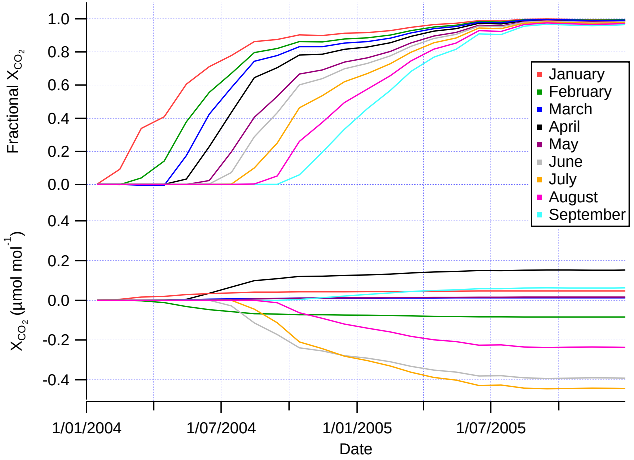

Fig. 13. The cumulative fractional X_{CO_2} change at Darwin due to pulse fluxes for each month from the Northern Hemisphere boreal terrestrial biosphere (top) and the changes observed in X_{CO_2} due to the optimized flux for each month.